Dual beam deflection of liquid crystal optical phased array

Fei Pan (潘 斐), Lingjiang Kong (孔令讲)*, Xiaobo Yang (杨晓波), Yue Ai (艾 越), and Yan Zhou (周 妍)

School of Electronic Engineering, University of Electronic Science and Technology of China, Chengdu 611731, China

**Corresponding author: lingjiang.kong@gmail.com*

Received May 24, 2012; accepted June 25, 2012; posted online December 20, 2012

Dual beam deflection models based on one dimensional liquid crystal optical phased array (LCOPA) are discussed and compared in this letter. The far-field diffraction performance of the models is influenced by various impact factors, such as fill factor and fringing electric fields. For optimizing far-field diffraction performance, the combined influence of different impact factors is analyzed and a phase iterative algorithm which use the root-mean-square (RMS) phase deviation as a performance index is presented. The proposed algorithm is able to reduce phase deviation and improve the performance of far-field diffraction pattern at the same time. The simulation and experiments used in the letter effectively verify the proposed algorithm.

OCIS codes: 050.1950, 230.3720, 120.5060, 230.1950.

doi: 10.3788/COL201210.S20502.

Optical phased array (OPA) is one technology which can be used for agile beam steering of laser phased array radar. Liquid crystal optical phased array (LCOPA) is widely used because of low energy consumption, affordable, lightweight, and random access[1−3]. In a one-dimensional (1D) LCOPA, a liquid crystal layer is electrically addressed by an array of narrow electrodes. A spatially periodic voltage profile can be applied to the electrodes to produce a spatially varying phase retardation across the aperture.

To improve throughput, multiple beams have been widely used in different areas, such as optical tweezers[4], optical communication[5], data storage[6] etc. Dual beam deflection models based on 1D LCOPA are discussed and compared by simulation and experiments in detail in this letter.

In practice, the far-field diffraction performance of dual beam deflection models is limited by the influence of fill factor, fringing electric fields[7], imperfect optical surfaces[8], Gaussian phases etc. In order to realize beam effective deflection and optimize the far field diffraction pattern, the combined influence of various impact factors are detailedly analyzed in the letter and a phase iterative algorithm which use the root-mean-square (RMS) phase deviation[9] as a performance index is presented. For validating the proposed algorithm, the corresponding simulations and experiments are carried out.

LCOPA is a kind of novel, programmable diffractive optical elements. It can be implemented using liquid crystals to produce phase shift. In a linear 1D LCOPA, the liquid crystal layer is electrically addressed by an array of long and narrow electrodes. By using periodic voltage profile, a sawtooth shaped index of refraction variation in the liquid crystal layer is produced. The effect as a prism is able to change the deflection of the beam like a blazed diffraction grating[10]. as shown in Fig. 1.

Figure 1 shows the traditional operation of an optical phased array. A linearly increasing phase front will steer a beam as if it passed through a physical prism. In order to reduce the response time and the thickness of the LC layer, a modulo 2π operation is applied to replacing the linearly increasing phase shift. So the sawtooth profile is produced like a blazed diffraction grating.

Figure 2 shows the model 1 of dual beam deflection. By using periodic ($N = N_1 + N_2$) triangle voltage profile, the phase shift in Fig. 2 can be produced.

Figure 3 shows the model 2 of dual beam deflection. By using two part approximate symmetrical periodic voltage, a spatially approximate symmetrical varying phase shift is produced across the aperture.

But in a real LCOPA, it is not easy to obtain the sawtooth phase profile (solid line) due to many impact factors. The realistic phase profile as the dashed curve in Figs. 1–3.

In order to analyze the models, simulations are carried out and the concrete parameters are set as follows. The

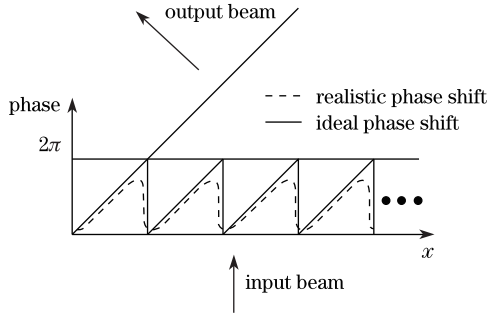

Fig. 1. Traditional phase profiles and beam steering of a LCOPA.

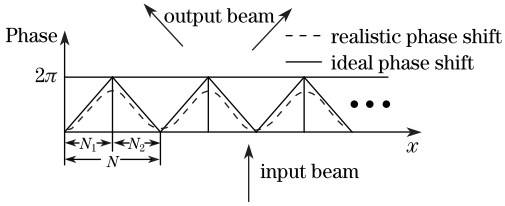

Fig. 2. Model 1 of dual beam deflection.

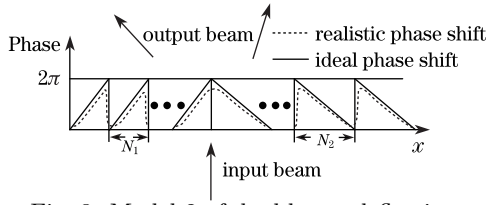

Fig. 3. Model 2 of dual beam deflection.

laser wavelength $\lambda = 0.6328$ μm, the center to center spacing between array elements $d = 5$ μm, the number of electrodes M=1 000, N_1 and N_2 are periods.

Figure 4 shows ideal far-field diffraction patterns of dual beam deflection models. It is obviously that besides the target diffraction orders, there appears some unexpected energy peaks in Fig. 4(a). Meanwhile, the beam can be steered effectively to the target in Fig. 4(b).

The corresponding experiments are carried out and Fig. 5 shows the experiment arrangement. Experimental facilities include a He-Ne laser source, a PC, a power source (5 V), a data line, and a beam control device. The beam control device consists of a control circuit and LCOPA. In the LCOPA, the liquid crystal layer is electrically addressed by 1000 electrodes. The laser wavelength $\lambda = 0.6328$ μm, the electrode width is 4 μm and the center to center spacing between array elements $d = 5$ μm.

In these experiments, the voltage commands are sent by PC. By using periodic voltage profile, a sawtooth shaped index of refraction variation in the liquid crystal layer is produced. So the output beam will be deflected. The far-field diffraction patterns are taken by the camera.

In Fig. 6(a), there are some unexpected diffract faculae. The experimental results are similar to the simulation results (Fig. 4(a)). Model 2 can well realize dual beam deflection. The energy mainly concentrates on target diffraction orders and 0st order, and a small amount of energy scattered in other orders.

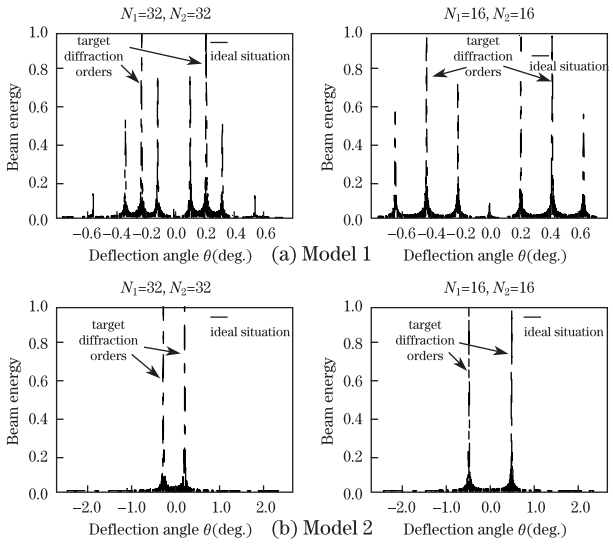

Fig. 4. Ideal far-field diffraction pattern of dual beam deflection models.

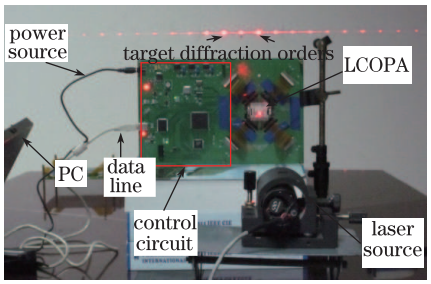

Fig. 5. Real scene of experiments.

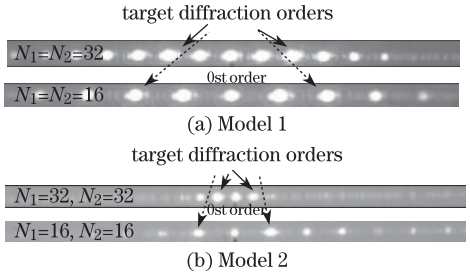

Fig. 6. Experimental results of dual beam deflection models.

Dual beam deflection models 1 and 2 are compared by simulation and experiments. In order to achieve better diffraction effect, the model 2 can be used.

In a real LCOPA, it is difficult to obtain the ideal sawtooth phase profile due to many impact factors. Because the performance of far-field diffraction is under the influence of impact factors, it will be necessary to analyze the impact factors and improve the performance of far-field diffraction.

The main impact factors include electrode fill factor (the ratio of the electrode width to the electrode spacing), fringing electric fields as Eqs. (1) and (2), manufacturing process error of optical surface in beam steering device as Eq. (3) and Gaussian random error etc.

$$\varphi(x) = \varphi_{\text{ideal}}(x) \otimes G(x), \tag{1}$$

where $\otimes$ denotes a convolution, φ is resulting phase shift, φ_{ideal} is the ideal phase, and G is a Gaussian kernel with 1/e width L[11] defined by

$$G(x) = \mathrm{e}^{-\frac{x^2}{L^2}}. \tag{2}$$

The fringing electric fields are caused by the voltage leakage between adjacent pixels electrodes. To simulate the effect of voltage leakage, it has been assumed that the effect on the phase distribution approximately corresponds to a convolution by a Gaussian kernel. For imperfect optical surfaces[8],

$$\varphi(x) = 2\pi A \cos\left[\frac{2\pi(x - x_{\text{midpoint}})}{d} - 0.5\right], \tag{3}$$

where A is one-half of the peak-to-valley amplitude of the undulation, x is the surface location, x_{midpoint} is the center of the aperture, d is the aperture diameter.

Figure 7 describes the detailed influence of different factors. Figures 7(a) and (b) show the change of reference phase shift. And the change of realistic phase shift is shown as Figs. 7(c) and (d). The fill factor is not 100%, so the fringing electric fields is unavoidable. Figure 7(c) shows the realistic phase shift after the influence of fringing electric fields. Moreover, manufacturing process error of optical surface in beam steering device and Gaussian random error cannot be ignored. At last, the realistic phase shift in Fig. 7(d) is a serious deviation from the ideal phase.

The simulation parameters are set as above. The laser wavelength $\lambda = 0.6328$ μm, the center to center spacing between array elements $d = 5$ μm, the number of electrodes M=1 000, N_1 and N_2 are periods. Meanwhile, fill factor is 80%, Gaussian kernel with $1/e$ width $L = 5$ μm, manufacturing process error $A = 0.1$ μm.

As shown in Figs. 8 and 9, in the realistic situation, the energy in target diffraction order is decreased and

scattered in other orders (compared with ideal situation) in the presence of impact factors. The energy in 0st order is second only to the target diffraction orders. If the beam steer to one direction, some energy will be focused on the opposite orders. So the energy in other orders (as shown in Fig. 9) is unavoidable in the dual beam deflection model.

The experiment arrangement is shown in Fig. 5. Experimental facilities include a He-Ne laser source, a PC, a power source (5 V), a camera, a data line and a beam control device. The number of electrode is 1 000. The laser wavelength $\lambda = 0.6328$ μm, the electrode width is 4 μm and the center to center spacing between array elements $d = 5$ μm.

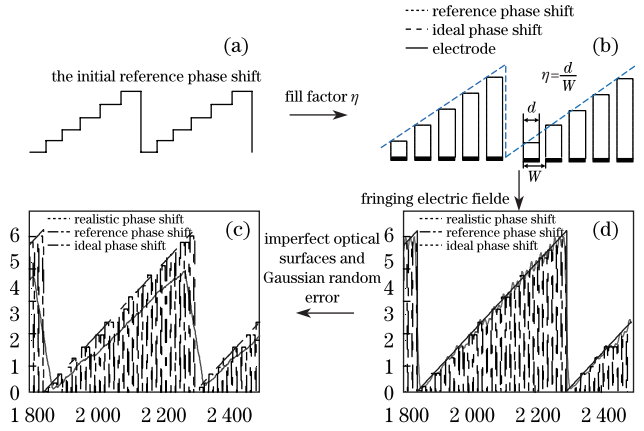

Fig. 7. Change of wavefront phase.

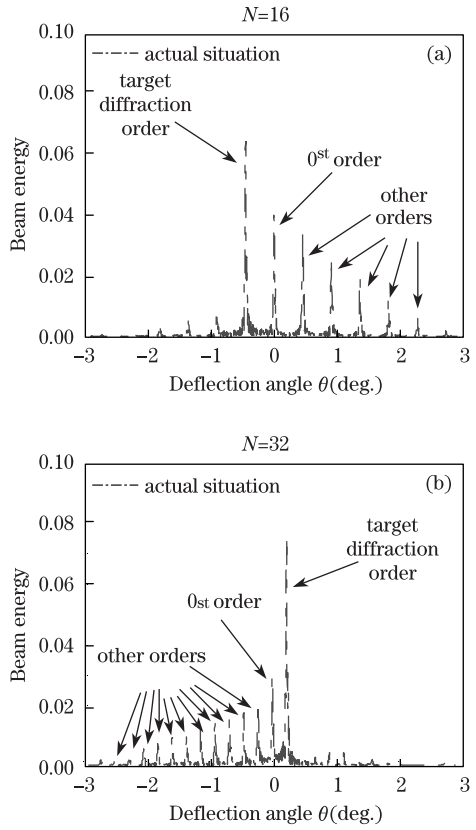

Fig. 8. Far-field diffraction pattern of traditional LCOPA model after combined influence.

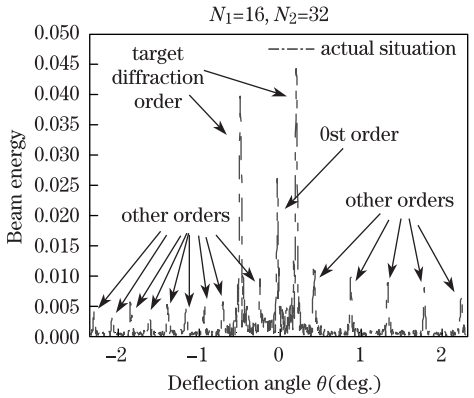

Fig. 9. Far-field diffraction pattern of dual beam deflection model 2 after combined influence.

Figure 10 shows relevant experiment results about Fig. 9. It is obvious that the diffraction light spots in target orders and 0st order are big and bright.

Model 2 can realize dual beam deflection effectively. A small amount of light still can't get effective deflection and concentrate on 0st order due to the existence of the impact factors. So the energy in 0st order must be reduced for optimizing the far field deflection performance.

Figure 11 shows the phase delay distribution. The reference phase is produced by an array of narrow electrodes, and voltage commands are applied to the electrodes.

Figure 12 shows response curve[12] for a nematic parallel-aligned liquid crystal cell ($\lambda = 0.6328$ μm). The liquid crystal molecules are birefringent. The molecules rotate when a voltage is applied, then the input beam produces different phase shifts[13]. Phase modulation, 0–7, can be addressed by proper electrode voltage command control.

Each iteration includes following steps:

1) According to Fig. 11, record the reference phase $\varphi_{\text{reference}}$ and the voltage command code of every electrode.

2) The impact factors result in distortion of the phase shift. Record the realistic phase $\varphi_{\text{realistic}}$,

3) Calculate root-mean-square phase deviation RMS_i as Eq. (4). The subscript i means iteration step i.

The root-mean-square phase deviation[9] can be described by

$$\text{RMS} = \sqrt{\frac{1}{M}\sum_{n=1}^{M}\left[\varphi_{\text{ideal}} - \varphi_{\text{realistic}}\right]^2}, \tag{4}$$

where φ_{ideal} is the ideal phase shift, $\varphi_{\text{realistic}}$ is the realistic phase shift, and M is the total number of electrodes. The smaller this value is the smaller the level of distortion is.

4) Sample the ideal phase shift and the realistic phase shift in the same position of horizontal direction, as shown in Fig. 13. Every electrode includes one sample point.

Calculate the phase difference as Eq. (5), then calculate the new reference phase shift as Eqs. (6–7),

$$\varphi_{\text{diff}} = \varphi_{\text{ideal\_sample}} - \varphi_{\text{realistic\_sample}}, \tag{5}$$

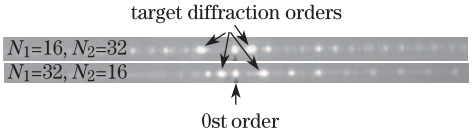

Fig. 10. Experimental results of Fig. 9.

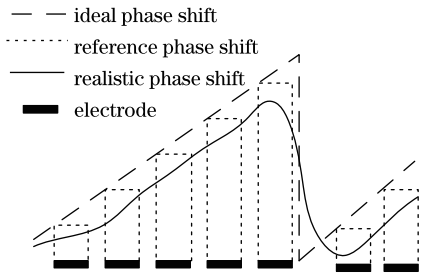

Fig. 11. Phase shift distribution.

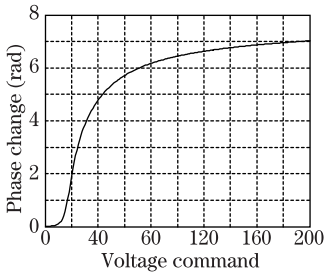

Fig. 12. Response curve for a nematic parallel-aligned liquid crystal cell.

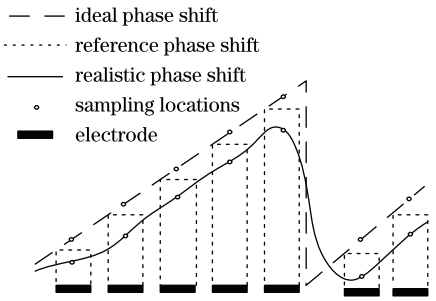

Fig. 13. Positions of sampling.

where $\varphi_{\text{ideal\_sample}}$ is the phase sampled from ideal phase shift and $\varphi_{\text{realistic\_sample}}$ comes from realistic phase shift. If $\varphi_{\text{diff}} > 0$, the $\varphi_{\text{realistic}}$ should increase in order to approach φ_{ideal}, and if $\varphi_{\text{diff}} < 0$, the $\varphi_{\text{realistic}}$ should decrease in order to approach φ_{ideal}.

$$\varphi'_{\text{reference}} = \varphi_{\text{diff}} + \varphi_{\text{reference}}. \tag{6}$$

Then

$$\varphi_{\text{reference}} = \varphi'_{\text{reference}}, \tag{7}$$

where $\varphi'_{\text{reference}}$ is the new reference phase shift. The reference phase shift results in realistic phase shift, and the new reference phase shift will come from response curve as shown in Fig. 12.

$$\varphi_{\text{curve\_min}} \leqslant \varphi_{\text{reference}} \leqslant \varphi_{\text{curve\_max}}, \tag{8}$$

and

if $\varphi_{\text{reference}} \leqslant \varphi_{\text{curve\_min}}$, then $\varphi_{\text{reference}} = \varphi_{\text{curve\_min}}$,

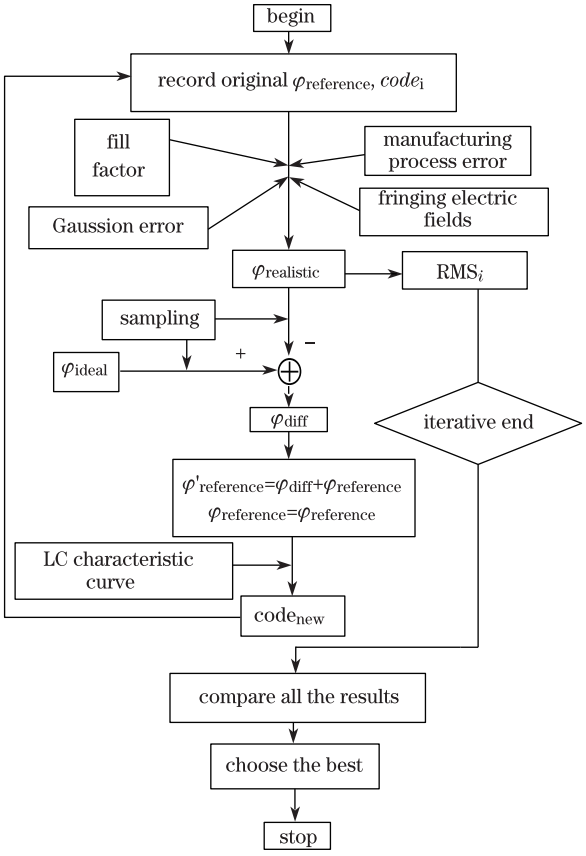

Fig. 14. Flowchart of the iterative algorithm.

if $\varphi_{\text{reference}} \geqslant \varphi_{\text{curve\_max}}$, then $\varphi_{\text{reference}} = \varphi_{\text{curve\_max}}$, where $\varphi_{\text{curve\_max}}$ and $\varphi_{\text{curve\_min}}$ represent the maximum and minimum phase shift of response curve (Fig. 12).

V. Search the new reference phase in the response curve as Fig. 12, then get the most suitable voltage commands code_{new} as the new voltage commands. Then compute the RMS phase deviation. After several iterations, compare the RMS phase deviation RMS, choose the voltage commands of minimum RMS.

The flowchart of the iterative is shown in Fig. 14.

The simulation parameters are set as above. The laser wavelength $\lambda = 0.6328$ μm, the center to center spacing between array elements $d = 5$ μm, the number of electrodes M=1 000, $N_1 = 16$, $N_2 = 32$ are periods. Meanwhile, fill factor is 80%, Gaussian kernel with 1/e width $L = 5$ μm, manufacturing process error $A = 0.1$ μm.

After several iterations, the voltage increase if the phase is too low and decreases if the phase is too high, and the realistic wavefront phase is close to the ideal phase shift.

As Fig. 16 shown, after optimized, the energy in 0st order and other orders is effectively reduced, especially the energy in 0st order.

The experiment arrangement and facilities are shown as above section. In Fig. 15, the voltage increases if the phase is too low and decreases if the phase is too high. Increase or decrease the voltage of the electrodes suitably in every period, then the far-field diffraction patterns can be optimized. The far field diffraction images are taken by the camera.

As Figs. 17 and 18 shown, it is clear that the laser

beam focus on the target diffraction orders after optimized, and targets have become more prominent. The experimental results show that this phase iterative algorithm is useful.

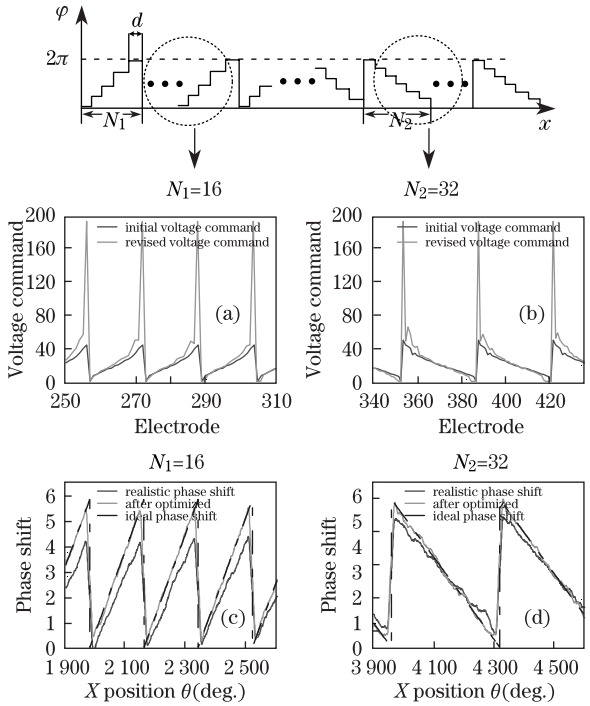

Fig. 15. Simulated results of the iterative algorithm.

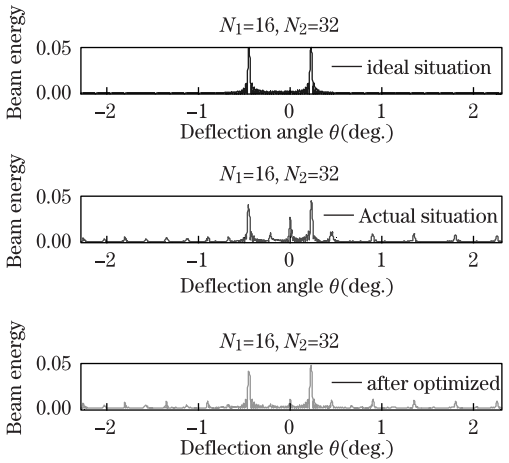

Fig. 16. Far-field diffraction patterns.

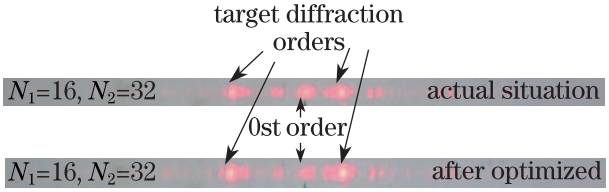

Fig. 17. Far-field diffraction patterns after optical filter

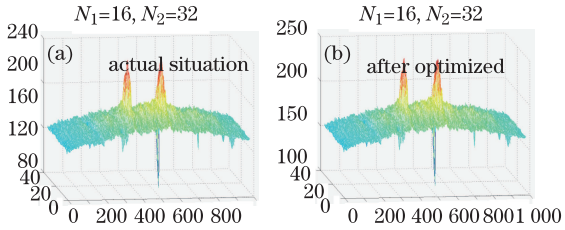

Fig. 18. Three-dimensional images of far-field diffraction patterns

Dual beam deflection models based on linear one dimensional LCOPA are discussed in the letter. Meanwhile, the models are compared by simulation and experiments and the model 2 is better than model 1. In reality, the performance of far-field diffraction is under the influence of various impact factors, the various impact factors are analyzed detailedly. Moreover, in order to realize beam effective deflection and improve the quality of far-field diffraction pattern, a performance optimization algorithm is presented. Finally, the corresponding simulation and experiments are used to prove the correctness and effectiveness of the algorithm.

This work was sponsored by National Natural Science Foundation of China (No. 61178068) and Sichuan Youth Science and Technology Foundation (No. 2011JQ0024).

References

1. P. F. McManamon, T. A. Dorschner, D. L. Corkum, L. J. Friedman, D. S. Hobbs, M. Holz, S. Liberman, H. Q. Nguyen, D. P. Resler, R. C. Sharp, and E. A. Watson, in *Proceedings of IEEE* **84,** 268 (1996).
2. P. McManamon, Proc. SPIE **5947,** 59470I (2005).
3. S. R. Harris, Proc. SPIE **4291,** 109 (2001).
4. V. Boyer, R. M. Godun, G. Smirne, D. Cassettari, C. M. Chandrashekar, A. B. Deb, Z. J. Laczik, and C. J. Foot, Phys. Rev. A **73,** 031402 (2006).
5. J. A. Anguita, M. A. Neifeld, and B. V. Vasic, Appl. Opt. **46,** 6561 (2007).
6. H.-F. Shih, Jpn. J. Appl. Phys. **44,** 1815 (2005).
7. U. Efron, B. Apter, and E. Bahat-Treidel, Proc. SPIE **5936,** 59360P (2005).
8. C. M. Titus, J. Pouch, H. D. Nguyen, F. Miranda, and P. J. Bos, Proc. SPIE **4825,** 177 (2002).
9. E. Hälstig, L. Sjövist, and M. Lindgren, Opt. Eng. **42,** 613 (2003).
10. S. R. Harris, Proc. SPIE **5162,** 157 (2003).
11. E. Haellstig, J. Stigwall, M. Lindgren, and L. Sjoqvist, Proc. SPIE **5087,** 13 (2003).
12. S. Serati and J. Stockley, in *Proceedings of Aerospace Conference 2002. IEEE* **3,** (2002).
13. L. Xu and Z. Huang, Proc. SPIE **7658,** 76580N (2010).